JOURNAL OF SOLID STATE CHEMISTRY 72, 257–271 (1988)

Structural, Optical, and Electronic Properties of Li_3MS_3 Compounds (M^{III} = Ti, Zr, Hf)

C. SOURISSEAU, S. P. GWET,* AND P. GARD

Laboratoire de Spectroscopie Moléculaire et Cristalline, UA 124 CNRS, Université de Bordeaux I, Talence Cedex 33405, France

AND Y. MATHEY†

Laboratoire de Spectrochimie des Éléments de Transition, UA420 CNRS, Université de Paris-Sud, Orsay 91405, France

Received January 21, 1987; in revised form May 22, 1987

The Li_3MS_3 powder samples (M^{III} = Ti, Zr, Hf), chemically prepared under mild conditions, have been studied by X-ray diffraction, infrared and Raman vibrational spectroscopies, UV–visible absorption, and electron paramagnetic resonance (EPR) technics. From X-ray data we confirm the topochemical mechanism of three lithium insertions into the 2D-MS_3 host lattices already proposed by R. R. Chianelli and M. B. Dines (*Inorg. Chem.* **14**, 2417 (1975)). From infrared and Raman results new structural information is obtained: on the one hand, the cleavage of $(S_2)^{2-}$ pairs induces a new arrangement of the basic structure and on the other hand, Li–S interactions are by far predominant within strongly distorted two LiS_4 and one LiS_6 groups; moreover M–S interactions are markedly weakened. From UV–visible and EPR spectroscopies, the electronic perturbations upon lithiation are evidenced: new d–d-type transitions, in the 550- to 660-nm range, and strong broad EPR signals suggest that M^{4+} (d^0) ions are transformed into M^{3+} (d^1) centers. In addition, some unpaired electrons, responsible for a narrow EPR line, appear to be localized around not totally ionized Li centers. Finally, a structural model, which takes into account all the above experimental results, is proposed; this model allows us also to explain the reactivity and some physical properties of the Li_3MS_3 phases when in short contact with air.

Introduction

Following the early works on lamellar dichalcogenides, the search for new compounds able to function as positive toward lithium intercalation in secondary batteries has led to a great number of chemical and electrochemical studies (*1–8*). In this respect, during the last decade, Dines and Chianelli (*9–11*) have described the reaction of *n*-butyllithium with layered transition metal trichalcogenides to yield lithiated products; they discovered that this reaction proceeds topochemically and leads to the formation of ternary phases of Li_3MS_3 general formula.

The group IV transition metal trichalcogenides have structures (*12, 13*) with chains of distorted trigonal M–X_6 prisms, infinitely

* Present address: Université de Yaoundé, Cameroon, Republic of Africa.

† Present address: Département de Physique, Faculté des Sciences de Luminy, Marseille Cedex 9 13288, France.

0022-4596/88 $3.00

extending parallel to the b axis of monoclinic cells; these chains occur in pairs with each member translated 0.5 unit cell. Chain pairs form a layered structure, the layers of which are separated by van der Waals gaps of polysulfide ions (Fig. 1). These MS_3 starting materials may be described as $M^{4+}(S_2)^{2-}S^{2-}$ and one can easily imagine that in Li_3MS_3 phases a reduction of both S_2^{2-} pairs and M^{4+} centers has occurred according to the following equation:

$$M^{4+}(S_2)^{2-}S^{2-} + 3Li^+ + 3e^- \rightarrow (Li^+)_3M^{3+}(S^{2-})_3.$$

However, from electrochemical discharge studies (*14, 15*) several authors have first suggested that a partially reversible mechanism could exist in the Li_xTiS_3 system and that three different reactional paths could occur:

(a) The starting MS_3 compound could decompose and transform into an MS_2 phase which would be electrochemically intercalated,

$$M^{4+}S_3 + 3Li^+ \xrightarrow{+3e^-} LiM^{3+}S_2 + Li_2S.$$

(b) Lithium diffusion could induce a new structural packing and lead to an octahedral coordination of the metal ions; the Li_3MS_3 compounds should thus crystallize into a $BaTaS_3$-type hexagonal system (*16*) with lithium ions occupying D_{3h} symmetry sites in between the "TaS_3" chains extending parallel to the c axis.

(c) Finally, a simple insertion mechanism of lithium ions could take place within the van der Waals gap, as it is well known for graphite compounds (*8*).

In contrast with the above assumptions, Chianelli and Dines (*10*) have shown from powder X-ray diffraction results and preliminary infrared data (mainly on Li_3TiS_3 because Li_3ZrS_3 and Li_3HfS_3 are very reactive and pyrophoric in air) that the trigonal prismatic $(MS_6)_\infty$ chains remain intact after lithium uptake, that only stoichiometric compounds are formed, and that the $(S{=}S)^{2-}$ bonds are broken on incorporation of lithium. However, these authors were not conclusive about the location of lithium ions in the surrounding of the chains. Actually, the diffusion mechanisms of these ions within the MS_3 lattices are still unknown and complete structural data are not yet available. Moreover, it is not easy to compare the Li_3MS_3 phases with the already known intercalated Li_xMS_2 compounds (*1–7*).

This study has thus been undertaken as a

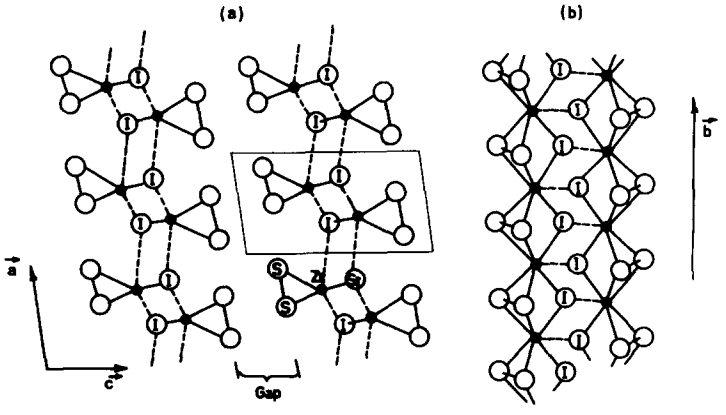

FIG. 1. Crystal structure of ZrS_3; (a) projection along (010) and (b) representation of two chains along the b-axis of the monoclinic structure.

part of a general vibrational and electronic study of two-dimensional compounds able to intercalate guest molecules or ions (*17–19*). Indeed, for these MS_3 semiconductors we have recently shown that infrared, Raman, and UV–visible spectroscopies yield a wealth of information about the structure and the dynamics of these host lattices (*10–22*). Furthermore, we have also recently investigated the infrared spectra of lithium intercalated phases in the Li_xMPS_3 (M^{2+} = Fe, Ni) and Li_xFeS_2 systems (*23, 24*) in order to determine the precise lithium surroundings and electronic transfers. We have thus carefully reexamined the Li_3MS_3 phases by X-ray diffraction, infrared and Raman spectroscopies, UV–visible absorption, and electron paramagnetic resonance (EPR) techniques in order to get a better insight into the structural and electronic perturbations upon lithium insertion and to draw more established conclusions about the diffusion mechanisms and the locations of Li^+ ions.

Experimental Section

Microcrystalline powders of MS_3 (M^{4+} = Ti, Zr, Hf) were obtained by heating stoichiometric amounts of metal and sulfur in sealed quartz tubes according to known procedures (*9–11*). When M = Zr or Hf, after several weeks under temperature, a large fraction of the material consisted of thin orange-red platelets grown by vapor phase self-transport; black platelets of TiS_3 were grown by chemical transport following a described procedure (*12, 13*).

Lithiation was carried out by treating the pure materials with a toluene solution of *n*-butyllithium for ~3 days at about 60°C in Pyrex ampoules sealed under vacuum. All operations were carried out under inert atmosphere using dry and desaerated solvents. The resulting solids were washed with toluene and then transferred into Lindeman, Pyrex, or quartz tubes for X-ray diffraction, Raman, and EPR spectroscopic analyses, respectively.

Pure and lithiated materials were characterized by chemical analyses and by means of X-ray diffraction using the Cu$K\alpha$ radiation with either a diffractometer or a Debye–Scherrer camera.

Infrared (600–200 cm^{-1}) and UV–visible transmission spectra (1200–250 nm) were recorded on the Perkin–Elmer 180 and 983 instruments and on a Cary 17 spectrometer using Nujol mulls. These measurements were performed at room temperature and at ~80 K using a homemade liquid nitrogen cryostat. No significant changes were noted on the low-temperature spectra and only the ambient temperature results will be reported and discussed. The Raman spectra were recorded on the Coderg T800 and Dilor RTI triple monochromators using the 647.1-nm exciting line of a Spectra-Physics Kr^+ Model 164 laser and the rotating sample technique in order to avoid any decomposition upon irradiation.

Finally, the EPR study was performed at X-band frequency with a Bruker ER 200D spectrometer equipped with a continuous helium flow cryostat, a Hall probe, and a frequency meter (0–6000 Gauss).

Results and Discussion

(*1*) *Reaction with n-Butyllithium and X-ray Diffraction*

Following the classical preparative route (*10*) we obtained black (M = Ti) or dark green (M = Zr, Hf) stoichiometric Li_3MS_3 compounds by reacting MS_3 with an excess of *n*-BuLi for about a week at room temperature or at 60°C. Our general observations about these reactions confirm those already reported by Chianelli and Dines (*10*). In addition we have observed that when adding BuLi in a ratio slightly smaller than or close to 3 : 1, with respect to the amount of MS_3, monophasic Li_xMS_3 compounds with $2 < x$

TABLE I

X-RAY POWDER DIFFRACTION PATTERNS OF HfS_3, Li_1HfS_3, Li_3HfS, AND A $Li_3HfS_{3(ox)}$ SAMPLE PARTIALLY OXIDIZED IN AIR[a]

HfS_3		Li_1HfS_3	Li_3HfS_3			$Li_3HfS_{3(ox)}$	Li_3HfS_3 (10)		
$d_{obs(int)}$	*hkl*	d_{obs}	$d_{obs(int)}$	d_{calc}	*hkl*	d_{obs}	$d_{obs(int)}$	d_{calc}	*hkl*
			11.14(m)	11.18	100	11.11			
8.9 (s)	001	8.95	9.16(s)	9.10	001	9.12	9.2(s)	9.1	001
		6.40	6.40(m)	6.40	101	6.42	6.5(m)	6.7	101
			5.58(w)	5.59	200	5.57	6.0(m)	5.9	200
5.05(w)	100								
6.47(w)	$10\bar{1}$								
4.46(w)	002	4.56	4.56(s)	4.55	002	4.55	4.57(s)	4.55	002
4.18(w)	101								
3.34(m)	011	3.33	3.40(w)	3.41	011	3.40			
3.15(w)	102		3.19(w)	3.19	111	3.19			
			3.03(w)	3.02	$21\bar{1}$	3.02	3.05(m)	3.07	$10\bar{3}$
				3.03	003			3.03	003
2.93(m)	110	2.93							
2.798(s)	012	2.80							
		2.617	2.617(s)	2.617	310	2.615	2.620(s)	2.632	$21\bar{2}$
2.522(m)	200	2.520	2.416(w)	2.414	212	2.415		2.631	$31\bar{1}$
				2.148	311				
2.346(m)	201	2.344							
2.288(w)	013								
2.227(w)	004								
2.146(w)	$10\bar{4}$								
2.067(m)	210	2.063							
1.962(m)	211	1.961							
1.893(w)	014								
			1.846(m)	1.846	313	1.846	1.847(m)	1.847	105
1.799(m)	021	1.797							

[a] Intensities are reported using s = strong, m = medium, w = weak, and the parameters of monoclinic cells are reported in the text and in Table II.

< 3 are yielded; the x values are then either close to 2.2–2.3 or close to 2.7–2.8 depending upon the reaction time and temperature. However, whenever less than 3 equivalents (i.e., 0.5, 1.0, or 2.0) of BuLi per equivalent of MS_3 is added, bicolored biphasic systems are preferentially formed rather than non-stoichiometric Li_xMS_3 ($0 < x \leq 2.0$) ternary phases. The identification of these biphasic products as mixtures of MS_3 (orange-red) and of Li_xMS_3 (green, $2.0 < x \leq 3.0$) was unambiguously carried out through X-ray powder diffraction (Table I, see first three columns) and vibrational spectrometry (see below).

Following the indexation previously proposed (*10*), X-ray powder diagrams of the fully lithiated products were interpreted on the basis of monoclinic unit cells. All the observed lines are broad indicating that diffusion of lithium ions has led to materials of relatively poor crystallinity. Nevertheless, again a rough correspondence can be established between the lattice parameters of the new black (M = Ti) or green (M = Zr, Hf) Li_3MS_3 phases (Table II).

The present sets of more complete data allow us not only to propose new values of lattice parameters but also to rule out definitively the formation of Li_2S (*14, 15*) and to confirm the topochemical mechanism already proposed by Chianelli and Dines (*10, 11*): after three Li^+ uptakes the bidimensional MS_3 structures expand largely along the *a* and *c* axes but they keep the original interchain arrangement almost unchanged (Fig. 1). The present data lead to expansion values slightly larger than those depicted previously. However, it is not yet clear whether or not the observed differences are ascribed to slightly different values of the nonstoichiometric coefficients *x* in the Li_xMS_3 formula; moreover, the absence of suitable single crystals after lithiation precludes the access to a more detailed structural description by X-ray diffraction methods. At this stage, it is impossible to localize precisely the Li^+ ions within the new structural packing of the reduced chains.

(2) Infrared and Raman Spectra

The infrared spectra (600–200 cm^{-1}) of the three MS_3 host lattices and of the corresponding Li_3MS_3 compounds at 300 K are compared in Fig. 2. Spectra of the lithiated products are quite simple and show tremendous changes when compared to those of the starting materials: all the bands due to the host lattices have disappeared and we observe only two sets of broad absorptions at about 450–410 cm^{-1} and 320–240 cm^{-1}. We propose to assign the higher frequency bands at 454 cm^{-1} in Li_3TiS_3, at 420 cm^{-1} in Li_3ZrS_3, and at 410 cm^{-1} in Li_3HfS_3 to stretching modes of "LiS_4" entities since similar band wavenumbers were encountered for Li^+ ions in tetrahedral surroundings in Li_2S (*10*) and Li_xFeS_2 phases (*24*). These modes probably involve lithium ions incorporated within the layers (in between the chains) where strong Li . . . S interactions are expected.

The remaining lower frequency bands are

TABLE II

LATTICE PARAMETERS IN MS_3 AND Li_3MS_3 MONOCLINIC STRUCTURES AND EXPANSIONS AS COMPARED WITH THE CORRESPONDING MS_3 COMPOUND[a]

Compounds		*a* (Å)	Δ2*a* (Å)	*b* (Å)	Δ*b* (Å)	*c* (Å)	Δ*c* (Å)	β (°)	Δβ (°)
TiS_3	(Ref. *13*)	4.96	—	3.40	—	8.78	—	97.3	—
	(Ref. *10*)	11.1 (1)	+1.2	3.46(1)	+0.06	9.12(2)	+0.34	98.0(2)	+0.7
Li_3TiS_3	(*)	11.29(3)	+1.37	3.44(2)	+0.04	9.54(2)	+0.76	105.1(1)	+7.8
ZrS_3	(Ref. *13*)	5.124	—	3.624	—	8.980	—	97.28	—
	(Ref. *10*)	11.2 (1)	+0.95	3.59(1)	−0.03	9.22(2)	+0.24	100.0(2)	+2.7
Li_3ZrS_3	(*)	11.45(1)	+1.20	3.69(1)	+0.07	9.27(1)	+0.29	101.9(1)	+4.6
HfS_3	(Ref. *13*)	5.092	—	3.595	—	8.967	—	97.38	—
	(Ref. *10*)	12.1 (1)	+1.92	3.52(1)	−0.07	9.24(2)	+0.27	100.0(1)	+2.6
Li_3Hf_S	(*)	11.46(1)	+1.28	3.68(1)	+0.09	9.33(1)	+0.36	102.7(1)	+5.3

Note. Asterisk denotes this work.

[a] Estimated standard deviations of the refined parameters are given in parentheses.

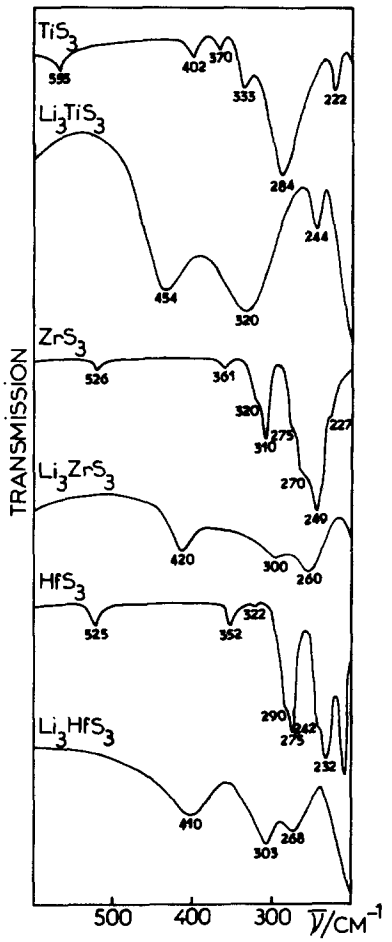

FIG. 2. Comparison of MS_3 and Li_3MS_3 infrared transmission spectra (600–200 cm^{-1}) at 300 K.

tentatively attributed to stretching vibrations of "LiS_6" groups since comparable wavenumbers were also reported for Li^+ ions in octahedral sites in $Li_4P_2S_6$ (335 cm^{-1}), Li_xFePS_3 (336 cm^{-1}), Li_xNiPS_3 (310 cm^{-1}), and Li_xFeS_2 (~320 cm^{-1}) compounds (*23, 24*). The large frequency splittings (35–75 cm^{-1}) indicate that these "LiS_6" entities must be markedly distorted as it is expected from structural considerations for Li^+ ions accommodated within the van der Waals gaps. It is noteworthy that the band at 244 cm^{-1} in Li_3TiS_3 has been previously reported at 225 cm^{-1} (*10*) and assigned to a Ti–S stretching vibration by comparison with the signals at 220 cm^{-1} in TiS_2 (*25*) and at 284–222 cm^{-1} in TiS_3 (*26*). Such a mode is expected to be metal dependent but we do not observe any counterpart in the spectra of Li_3ZrS_3 and Li_3HfS_3. We thus conclude that Li . . . S interactions are by far predominant in the Li_3MS_3 phases and that vibrations involving M^{3+} ions must only appear in the low-frequency region ($\nu < 200$ cm^{-1}) as previously noted in MPS_3 and Li_xMPS_3 compounds (*18, 23*).

The Raman spectra of several lithiated products of HfS_3 with various lithium contents, namely $Li_{0.0}HfS_3$, $Li_{0.5}HfS$, $Li_{2.0}HfS_3$, $Li_{3.0}HfS_3$, and those of partially and completely oxidized Li_3HfS_3 samples, are shown in Fig. 3. Similar but less complete Raman results obtained for the Li_xZrS_3 system are reported in Fig. 4. The corresponding Raman band wavenumbers of Li_3ZrS_3 and Li_3HfS_3 compounds are gathered in Table III. Unfortunately, Raman experiments on Li_xTiS_3 samples were not successful due to the high reflectivity and opacity of these dark samples. So, we shall

TABLE III

INFRARED (IR) AND RAMAN (R) BAND WAVENUMBERS (cm^{-1}) IN Li_3MS_3 COMPOUNDS (M^{3+} = Ti, Zr, Hf) AT 300 K AND TENTATIVE ASSIGNMENTS (a AND b)

Li_3TiS_3	Li_3ZrS_3		Li_3HfS_3		Assignments[a]	
IR	IR	R	IR	R	a	b
		440 m		430 m		$\nu_{asym}LiS_4$
454 s	420 s		410 s		ν LiS_4	$+LiS_6$
		375 vs		377 vs		$\nu_{sym}LiS_4$
		320 m		320 m		
320 s	300 s		303 s		ν LiS_6	$+LiS_6$
		265 w		280 w		
244 m	260 s		268 s			
		214 m		216 m	δ SLis	δ SLiS
		184 m		190 w		
		134 m		126 m	$\nu M-S_6$	$\nu(M-S)$
		113 w		110 m		
		74 m		58 m		$T'(M^{3+})$

[a] See text.

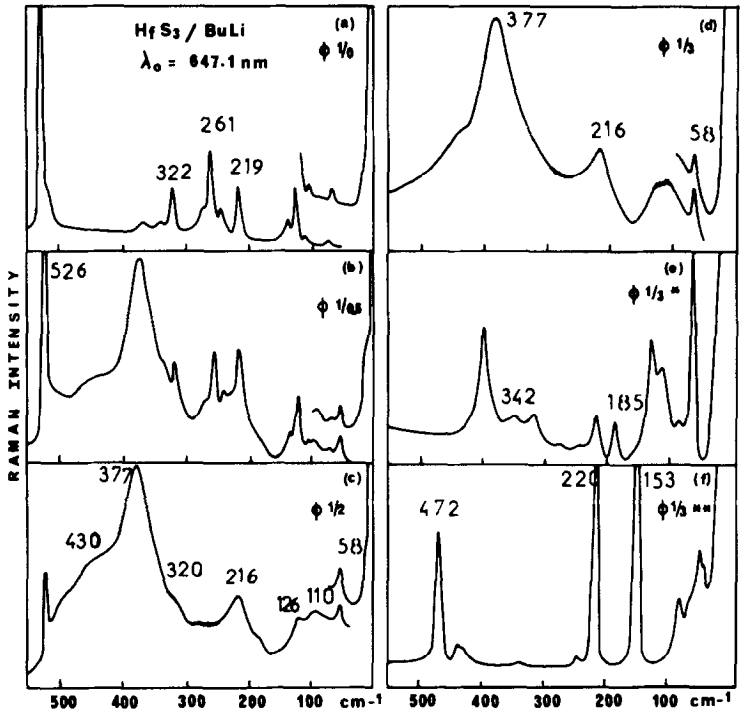

FIG. 3. Raman spectra (550–10 cm^{-1}) of HfS_3 and of several Li_xHfS_3 lithiated solid compounds prepared according to various HfS_3/nBuLi ratios (ϕ): (a) HfS_3, (b and c) mixtures of HfS_3 and Li_3HfS_3, (d) Li_3HfS_3, (e) Li_3HfS_3 partially oxidized after a short contact in air, (f) Li_3HfS_3 completely oxidized after a long contact in air.

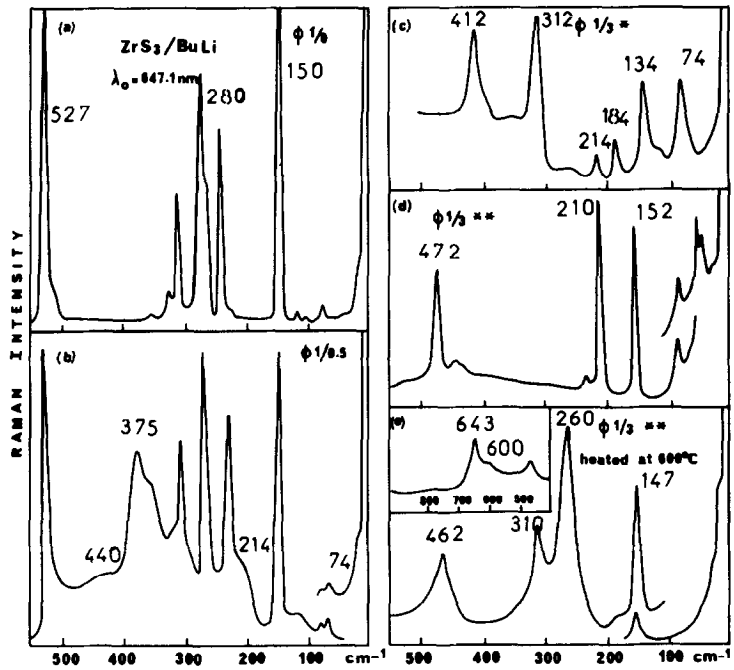

FIG. 4. Raman spectra (550–10 cm^{-1}) of ZrS_3 and of several Li_xZrS_3 lithiated solid phases (same key as in Fig. 3).

mainly discuss the more complete results obtained with the hafnium derivatives. As the x value increases the Raman spectra of Li_xHfS_3 samples (Figs. 3a–3d) are essentially a juxtaposition of decreasing thin bands due to the HfS_3 lattice and of increasing broad bands due to the final Li_3HfS_3 phase: these results are in perfect agreement with X-ray and infrared observations which have indicated that nonstoichiometric compounds do not exist. It is noteworthy that the intense signal at 526 cm^{-1} due to the stretching vibration of S_2^{2-} pairs has completely disappeared on the Li_3HfS_3 spectrum, a result in agreement with previous infrared results (*10*). We conclude that there is a cleavage of $(S{=}S)^{2-}$ bonds and a reduction of S_2^{2-} pairs upon incorporation of lithium. Considering now the Raman spectrum of Li_3HfS_3, one can distinguish three groups of broadbands in the 430–280 cm^{-1}, 220–180 cm^{-1}, and 130–50 cm^{-1} frequency regions, respectively:

(a) The higher frequency signals can be assigned to Li–S stretching vibrations of LiS_4 and LiS_6 entities as above discussed in the infrared results (Table III (a)); some bands are overlapping but the maximum at 377 cm^{-1} is a good candidate for the $\nu_{sym}(LiS_4)$ vibration of tetrahedral groups.

(b) The second group of bands is likely to be due to δ(S–Li–S) deformation modes since it is not metal sensitive (Table III).

(c) Finally, the third group of bands appears metal dependent and it is assigned to $\nu(M{-}S_6)$ type vibrations. It is noteworthy that the last thin Raman band is observed at 58 cm^{-1} in Li_3HfS_3 and at 74 cm^{-1} in Li_3ZrS_3 leading to the highest metal dependency; this vibration probably corresponds to large amplitude vibrational motions of the Hf^{3+} and Zr^{3+} ions.

We thus conclude that $M{-}S_6$ interactions are markedly perturbed and weakened while Li–S bondings are favored in Li_3MS_3 compounds. A new electronic distribution results from these materials as compared with the starting host lattices. On the one hand, the cleavage of polysulfide bonds has induced a rearrangement of the basic structure and on the other hand a complex distribution of Li–S distances must appear since the Raman spectra of Li_3MS_3 phases are poorly resolved and look like those of statistically disordered systems.

In sharp contrast with this last observation, Li_3HfS_3 (Fig. 3e) and Li_3ZrS_3 (Fig. 4c) samples partially oxidized in air give rise to nicely resolved Raman bands at nearly the same wavenumbers and with similar relative intensities excluding the very low-frequency metal-dependent bands which are markedly enhanced. Surprisingly, the crystal structures of Li_3MS_3 phases become more ordered after a very short contact with air. Later, after a complete oxidation process, one obtains only products of decomposition as evidenced by the drastic spectroscopic changes (Figs. 3f and 4d) and the resulting Raman spectra are now characteristic of polysulfides (*27–28*).[1]

All these new vibrational results allow us to conclude that the MS_3 host lattices may accommodate three lithium ions with great structural distortions. We can definitely rule out a localization of all Li^+ ions within the van der Waals gap and the existence of a simple intercalation as in graphites. Furthermore, a concerted displacive mechanism on metal ions to occupy centrosymmetric sites, as in a $BaTaS_3$ structure, does not take place. Finally, we have noted an

[1] The observed resonance Raman enhanced spectra of these polysulfides do not allow us to detect the probable formation of MO_2 oxides as expected. So, we have intentionally exposed to the air an oxidized sample of Li_3ZrS_3 at 600°C in order to make easier the complete substitution of sulfur by oxygen atoms. The Raman spectrum of the ZrO_2 oxide has thus been readily obtained (Fig. 4e); surprisingly, it is a fingerprint of zirconia in its tetragonal structure (*29, 30*) a phase generally difficult to stabilize under so mild conditions (*31*).

ordering of the Li_3MS_3 structures upon a slight oxidation of crude reaction products.

(3) UV–Visible Spectra and EPR Results

The UV–visible (250–1200 nm) transmission spectra of MS_3 and Li_3MS_3 solid compounds under study are compared in Fig. 5. It is noteworthy that the intense bands due to excitonic-type transitions at 963, 507, and 453 nm in TiS_3, ZrS_3, and HfS_3, respectively (*20–22, 32, 33*), completely disappear upon lithiation. In agreement with the mentioned color changes, Li_3MS_3 compounds are less absorbing materials in the visible region but they still exhibit absorption edges characteristic of broadband semiconductors. Now, the new relatively weak transitions detected in the 550- to 560-nm range could be due to *d–d*-type electronic transitions suggesting that the reduction process has modified the electronic density on the metal centers and transformed M^{4+} (d^0) ions into M^{3+} (d^1) centers. In another respect, due to their energy location and relative high intensity, the bands observed at 340–300 nm are assigned to sulfur-to-metal charge transfer transitions: this indicates again that lithiation has induced several electronic perturbations of the host lattices. In order to get a better understanding of these effects and in addition to a theoretical study based upon EHTB calculations, which is underway (*34*), we have investigated the Li_3MS_3 phases by EPR spectroscopy.

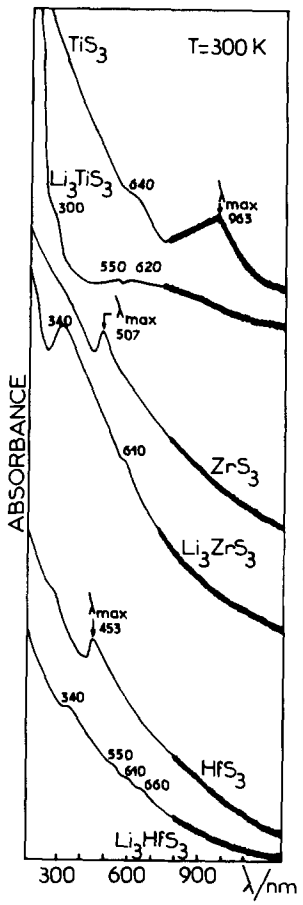

FIG. 5. Comparison of the UV–visible transmission spectra (250–1200 nm) of MS_3 and Li_3MS_3 solid compounds at 300 K. (Maxima of the excitonic transitions, λ_{max}, in the MS_3 spectra are indicated by arrows.)

The *X* band EPR spectrum of a fully lithiated microcrystalline powder sample of Li_3ZrS_3 at 290 K is shown in Fig. 6. A single broad nearly isotropic line, with $g \sim 2.11$ and a peak to peak width $\Delta H = 800$ G, is observed. As detected on traces b to e of Fig. 6, upon cooling a new narrow line ($\Delta H = 200$ G at 100 K) appears in the region between the two wings of the first broad line. This new component, centered at $g \sim 1.98$, remarkably increases at low temperature while the broad component continuously broadens and disappears at 4.2 K (Fig. 7).

A similar unexpected behavior is also observed upon cooling Li_3TiS_3 and Li_3HfS_3 systems (Figs. 8 and 9). In some instances, particularly after reduction of the MS_3 powder in the presence of a large excess of butyllithium, an additional very narrow line centered around $g \sim 2.00$ was also detected. Although rather weak, this third component never completely disappeared from the spectra of Li_3TiS_3 and Li_3HfS_3 even after repeated and careful washings

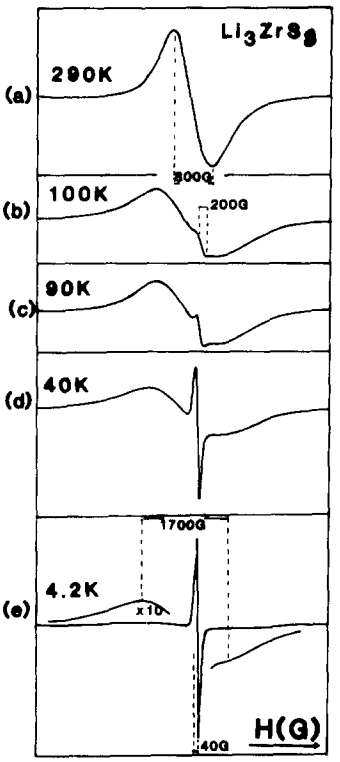

FIG. 6. EPR spectra of a Li_3ZrS_3 solid sample at various temperatures.

and annealings: this feature is confidently assigned to the presence of a very small amount of unreacted reducing agent or to some derived radicals; its superimposition does not modify the overall aspect of the other experimental lines.

Finally, in the particular case of Li_3HfS_3 a rather well-defined structure with four equal absorption lines has been detected at below 100 K in the central part of the spectra; the splitting between each neighboring line is estimated at about 68 G (see inset in Fig. 9).

At first glance, the general shape and behavior of the reported spectra do not conform to those expected for nd^1 species, even in distorted environments. As a matter of fact, it is rather puzzling to detect two superimposed lines which behave in a very distinct manner upon lowering the temperature when only one kind of unpaired electrons, i.e., those which half-fill the dz^2 levels or bands of the transition metal centers, is expected. However, such a situation has already been encountered by Kanzaki *et al.* (*35*) in the EPR spectrum of layered transition metal dichalcogenides intercalated by alkali ions. Referring to this paper, one can assign the strong broad components to $(dz^2)^1$ electrons almost localized on low symmetry transition metal sites in the reduced chains while the other narrow components could correspond to electrons located at or near the not totally ionized lithium centers. This last assignment is supported by two experimental observations:

(a) The weak intensity of the narrow component indicates that it is connected to a relatively small fraction of the total number of unpaired electrons as can be expected for the electronic density still located on lithium centers.

(b) The tetrafold structure superimposed to the central line in the low-temperature spectra of Li_3HfS_3 (Fig. 9) demonstrates the existence of a hyperfine interaction involving the nuclear spins ($I = \frac{3}{2}$) of ^7Li centers located close to the reduced chains.

Now, as indicated by the experimental value of the hyperfine splitting parameter (~190 MHz) compared to the tabulated isotropic hyperfine coupling constant A_0 for ^7Li (402 MHz (*36*)), this interaction is rather important. It is more likely, therefore, that the interacting electrons are in the immediate vicinity of Li nuclei (either in the bulk or in surface species) rather than in a largely delocalized electronic cloud around the reduced transition metals. It is emphasized that this structure (superhyperfine in nature), opportunately observed in the hafnium derivative, strongly helps us to propose an assignment rather questionable otherwise; we assume also that such an assignment can be applied to the other systems under study.

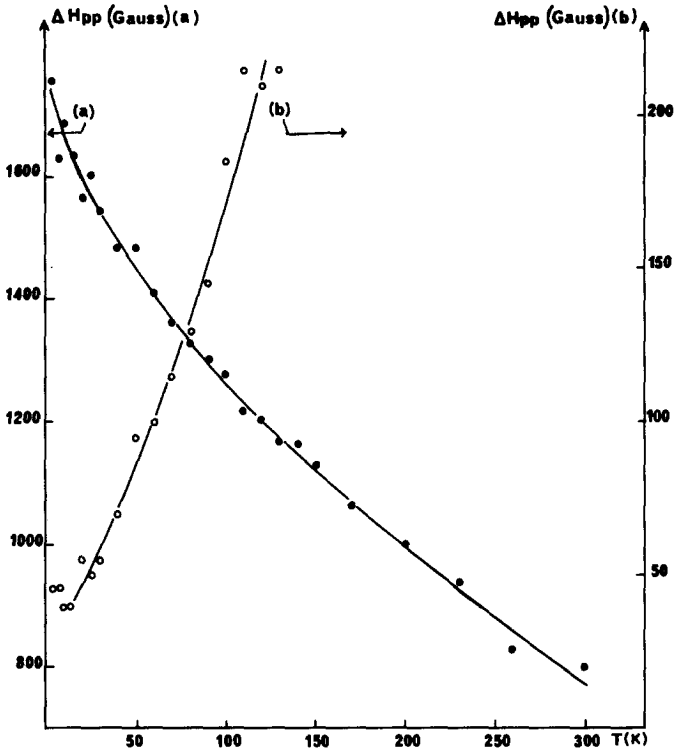

FIG. 7. Temperature dependences of the peak to peak widths (ΔH_{pp}) of the two EPR lines observed in Li_3ZrS_3.

Considering now the main broad component of the spectra, its progressive broadening from about 800 G at 290 K to about 1700 G at 4 K is still unexplained (Fig. 7). Variable temperature magnetic susceptibility measurements, carried out on a Li_3ZrS_3 sample, clearly indicate, however, that this reduced system strictly follows a Curie Law above 50 K (*37*); therefore, the corresponding unpaired electrons are not antiferromagnetically coupled and no exchange-broadening mechanisms involving nearest d^1 centers in the chains can be invoked to account for the observed phenomenon. Under these conditions, we describe this seldom linewidth behavior to dipolar interactions between neighbor paramagnetic centers and to unresolved hyperfine interactions.

Despite several uncertainties due to perhaps inhomogeneity and impurity problems, the major point raised by this EPR study is that after lithium insertion and accommodation of electrons in these 2D-MS_3 host lattices, some unpaired electrons appear to be rather localized around Li centers. These electrons are responsible for a narrow resonance line distinguishable from the broad line ascribed to the larger proportion of electrons effectively transferred to the host system. The coexistence of these two types of lines over the almost complete 4–300 K temperature range suggests also that, even at room temperature, electron exchange (if any) is slow between the two kinds of sites. The electrons that form the narrow line are therefore unlikely to be involved in a partially reversible process.

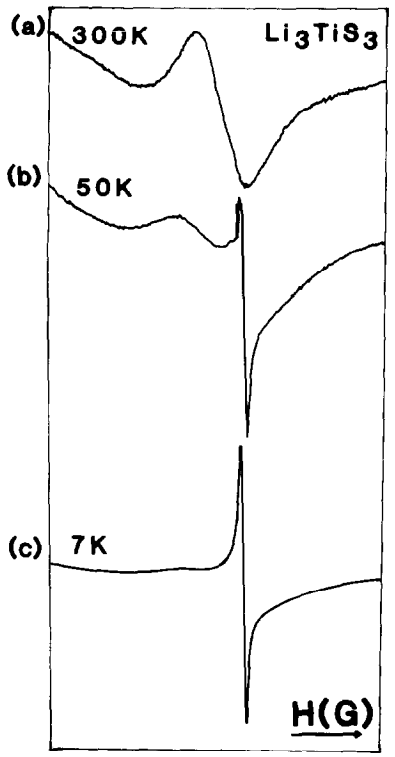

FIG. 8. EPR spectra of a Li_3TiS_3 solid sample at various temperatures.

Further studies on similar Na_xMS_3 phases are now in progress to clarify these electronic perturbations.

Lithium Diffusion, Structural Model, and Concluding Remarks

From the above experimental results, one can imagine a simple mechanism of diffusion for lithium ions in between the chains and within the van der Waals gaps of the MS_3 structure. We have thus tentatively searched for approximate positional parameters of Li^+ ions, maximizing Li–S interactions and minimizing M . . . S, Li . . . Li, and Li . . . M interatomic contacts, and we have tried to get information about the bondings and distortions within the "LiS_4" and "LiS_6" possible surroundings. In such a calculation performed on Li_3ZrS_3 (Table IV), all the y/b values found in ZrS_3 were fixed since no expansion of the b parameter was observed. The positions of sulfur atoms in the ac planes were changed in order to increase intrachain and interchain Zr–S distances in agreement with the observed expansions of a and c parameters: Zr–S bond distances thus increase from ~2.60 Å in ZrS_3 to 2.73 Å ($Zr–S^I$) or 3.08 Å ($Zr–S^{II}$) in Li_3ZrS_3; meanwhile, due to the cleavage of $(S_2)^{2-}$ pairs, S^{II} . . . S^{II} distances increase from 2.09 to 2.90 Å ($a/4$). Therefore, two first sets of lithium atoms were localized in between the chains giving rise to distorted LiS_4 ("T_d sites") entities and the third set was located on gap edges leading to strongly distorted LiS_6 ("O_h

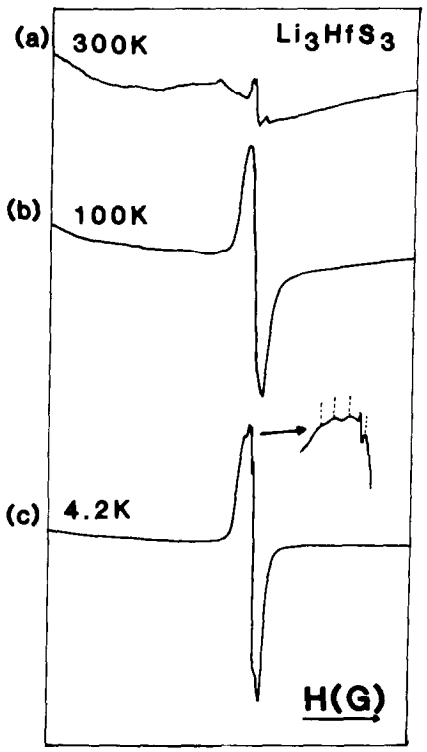

FIG. 9. EPR spectra of a Li_3HfS_3 solid sample at various temperatures; the inset shows the tetrafold structure superimposed to the central line.

TABLE IV

POSITIONAL PARAMETERS IN THE PROPOSED MONOCLINIC STRUCTURE OF Li_3ZrS_3

Atom[a]	2x	y	z
1 Zr	+0.250	+½	−0.140
2 Zr	−0.250	0	+0.140
3 S^{II}	+0.426	0	−0.360
4 S^{II}	−0.074	0	−0.360
5 S^{I}	+0.309	0	+0.082
6 S^{II}	−0.426	+½	+0.360
7 S^{II}	+0.074	+½	+0.360
8 S^{I}	−0.309	+½	−0.082
9 Li	+0.0	+½	+0.082
10 Li	+0.0	+0	−0.082
11 Li	−0.324	+½	−0.360
12 Li	+0.324	0	+0.360
13 Li	−0.50	0	−0.082
14 Li	−0.50	+½	+0.082

[a] The numbering of atoms is done according to Fig. 10.

sites") groups (Table III and Fig. 10). Under these assumptions the resulting topology implies that significant and quite comparable Li . . . S interactions exist within the Li (T_d) . . . S_4 and Li (O_h) . . . S_6 groups.[2] It is obvious that such a simple structural model does not take into account the doubling of the *a* parameter in Li_3ZrS_3; this probably comes from a slight displacement of the chains and/or a nonconcerted rotation of these chains about the *b* axis. Nevertheless, this approach allows us to propose a more realistic assignment of the vibrational spectra (Table IV) which takes into account the following arguments:

(a) Bands due to the two LiS_4 groups and to the LiS_6 entity are no more distinguished and are probably overlapping.

(b) The corresponding antisymmetric and symmetric stretching modes now correspond to intense infrared and Raman signals, respectively.

(c) As expected, bandwave numbers due to *M*–S stretching modes are markedly lowered and localized in the low-frequency region ($\nu \leq 140$ cm^{-1}).

Interestingly, we can also suggest a tentative assignment for the additional bands at 350–340 cm^{-1} and at 185 cm^{-1} on the Raman spectra of Li_3MS_3 samples in short contact with air: these bands could correspond to ν(Li–Li) vibrations since the interlithium distances are estimated equal to 2.40–2.90 Å for Li(T_d)–Li(T_d) and to 3.38–3.52 Å for Li(T_d)–Li(O_h) nearest contacts. These values can be nicely compared with those already known for Li_2 species in the

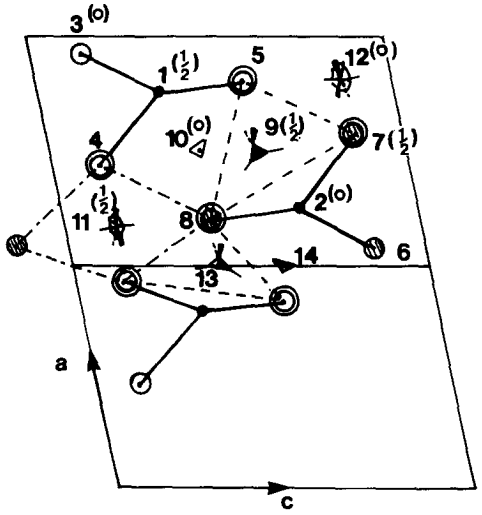

FIG. 10. Projection along (010) of the proposed monoclinic structure for Li_3ZrS_3: ●, Zr^{3+}; ○, S^{2-}; △, Li^+ in "T_d sites"; and ◯ Li^+ in "O_h sites"; positional parameters are reported in Table IV.

[2] In LiS_4 groups, Li–S distances are varying from 2.08 to 2.57 Å with average distances equal to 2.23 Å around $Li_{(13)}$ or $Li_{(14)}$ ions and equal to 2.44 Å around $Li_{(9)}$ or $Li_{(10)}$ ions (as compared with 2.35 Å in Li_2S). In LiS_6 entities one finds four similar short Li–S distances of 2.35 Å and two relatively larger ones of 2.54–2.57 Å leading to an average small value of 2.42 Å (as compared with 2.5–2.6 Å generally encountered in LiS_6 environments). It is also noteworthy that this simple structural model could be optimized since some Li . . . Zr distances are still relatively small (see [$Li_{(9)}$ . . . $Zr_{(1)}$] = 2.78 Å, [$Li_{(9)}$ . . . $Zr_{(2)}$] = 2.48 Å, [$Li_{(13)}$ . . . $Zr_{(2)}$] = 2.24 Å, and [$Li_{(14)}$ . . . $Zr_{(2)}$] = 2.33 Å).

ground state (2.67 Å–351 cm^{-1}) and in the first excited state (3.55 Å–227 cm^{-1}) (*38, 39*) but a partial clustering of lithium on tetrahedral sites to form Li_3 could also be invoked (*40*). Therefore, from the above EPR results, it appears that the existence of not totally ionized lithium atoms could initiate the formation of Li_2 or Li_3 species when the samples are in contact with air traces although the chemical process of such a reaction is still unexplained. It is noteworthy that the surprising ordering of the Li_3MS_3 crystal structures, as evidenced by the drastic sharpening of all the Raman bands (Figs. 3 and 4), seems correlated with the formation and stabilization of these lithium dimers or trimers.

Obviously, new investigations of these systems, in particular using $^7Li/^6Li$ isotopic substitutions and using NMR experiments, could help us to obtain complementary structural data. Presently, we definitively conclude that Li–S interactions are predominant in the Li_3MS_3 phases which contain two kinds of lithium ions in LiS_4 and LiS_6 environments, while *M*–S interactions are markedly weakened.

Complementary electrochemical desintercalation studies of the Li_3MS_3 materials should also provide new information about the occupation rates of Li^+ ions in the different sites and about the domains of existence of "Li_xMS_3" positives so far generated.

Acknowledgments

The authors are thankful to Professor R. Brec and to Dr. O. Gorochov for discussions during the course of this work. S.P.G. is most appreciative to the Cameroon government for a stipend while this work was initiated. The authors are also indebted to the referees for critical reading of the manuscript and fruitful comments about the structural model.

References

1. J. Rouxel, *J. Solid State Chem.* **18,** 9 (1976).
2. D. W. Murphy, C. Cros, F. J. Disalvo, and J. V. Waszczak, *Inorg. Chem.* **16,** 3027 (1977).
3. M. S. Whittingham, *Prog. Solid State Chem.* **12,** 41 (1978).
4. A. J. Jacobson, M. S. Whittingham, and S. M. Rich, *J. Electrochem. Soc.* **126,** 887 (1979).
5. T. Jacobsen, K. West, and S. Atlung, *Electrochem. Acta* **27,** 1007 (1982).
6. (a) R. Brec, G. Ouvrard, A. Louisy, J. Rouxel, and A. Le Mehaute, *Solid State Ionics* **6,** 185 (1982). (b) J. Rouxel and R. Brec, *Annu. Rev. Mater. Sci.* **16,** 137 (1986).
7. A. Dugast, R. Brec, G. Ouvrard, and J. Rouxel, *Solid State Ionics* **5,** 375 (1981).
8. See reference *in* "Springer Series in Solid State Sciences" Vol. 38 "Physics of Intercalation Compounds" (L. Pietronero and E. Tosatti, Eds.), Springer-Verlag, Berlin (1981).
9. M. B. Dines, *Mater. Res. Bull.* **10,** 287 (1975).
10. R. R. Chianelli and M. B. Dines, *Inorg. Chem.* **14,** 2417 (1975).
11. R. R. Chianelli, *J. Crystal Growth* **34,** 239 (1976).
12. W. Kronert and K. Plieth, *Z. Anorg. Chem.* **336,** 207 (1965).
13. S. Furuseth, L. Brattas, and A. Kjekshus, *Acta Chem. Scand. A* **29,** 623 (1975).
14. M. S. Whittingham, *J. Electrochem. Soc.* **123,** 315 (1976).
15. D. W. Murphy and F. A. Trumbore, *J. Electrochem. Soc.* **123,** 960 (1976).
16. R. A. Gardner, M. Vlasse, and A. Wold, *Inorg. Chem.* **12,** 2784 (1979).
17. Y. Mathey, R. Clement, C. Sourisseau, and G. Lucazeau, *Inorg. Chem.* **19,** 2773 (1980).
18. C. Sourisseau, J. P. Forgerit, and Y. Mathey, *J. Solid State Chem.* **49,** 134 (1983).
19. O. Poizat and C. Sourisseau, *J. Phys. Chem.* **88,** 3007 (1984).
20. C. Sourisseau and Y. Mathey, *Chem. Phys.* **63,** 143 (1981).
21. S. P. Gwet, Y. Mathey, and C. Sourisseau, *Phys. Status Solidi B* **123,** 503 (1984).
22. P. Gard, F. Cruege, C. Sourisseau, and O. Gorochov, *J. Raman Spectrosc.* **17,** 283 (1986).
23. M. Barj, C. Sourisseau, G. Ouvrard, and R. Brec, *Solid State Ionics* **11,** 179 (1983).
24. P. Gard, C. Sourisseau, G. Ouvrard, and R. Brec, *Solid State Ionics* **20,** 231 (1986).
25. J. E. Smith, M. I. Nathan, M. W. Shaffer, and J. B. Torrance, *Proc. Int. Conf. Phys. Semicond., 11th,* **2** 1306 (1972).
26. G. Perrin, A. Perrin, and J. Prigent, *Bull. Soc. Chim. Fr.* **8,** 3086 (1972).
27. R. Steudel, *Angew. Chem. Int. Ed. Engl.* **14,** 655 (1975).

28. C. DOMINGO AND S. MONTERO, *J. Chem. Phys.* **74,** 862 (1981).
29. D. MICHEL, M. P. JORBA, AND R. COLLONGUES, *J. Raman Spectrosc.* **5,** 163 (1976).
30. C. H. PERRY, D. W. LIU, AND R. P. INGEL, *J. Amer. Ceram. Soc.* **68,** C184 (1985).
31. Y. C. ZHANG, S. DAVISON, R. BRUSACO, Y. J. QIAN, K. DWIGHT, AND A. WOLD, *J. Less-Common Met.* **116,** 301 (1986).
32. W. SCHAIRER AND M. W. SCHAFER, *Phys. Status Solidi A* **17,** 181 (1973).
33. S. KURITA, J. L. STAEHLI, M. GUZZI, AND F. LEVY, *Physica B* **105,** 169 (1981).
34. C. THIEFFRY, E. CANADELL, Y. MATHEY, AND M. WHANGBO, to be published.
35. Y. KANZAKI, S. OGURA, O. MATSUMOTO, AND Y. TOIDA, *Physica B* **114,** 379 (1982).
36. J. E. WERTZ AND J. R. BOLTON, "Electron Spin Resonance: Elementary Theory and Practical Applications," McGraw–Hill, New York (1972).
37. Y. MATHEY, unpublished results (data available upon request).
38. R. A. BERNHEIM, L. P. GOLD, P. B. KELLY, T. TIPTON, C. A. TOMCZYK, AND D. K. EIRS, *in* "Springer Series in Optical Sciences: Laser Spectroscopy," Vol. 30, p. 122, Springer-Verlag, Berlin (1981).
39. G. IGEL-MANN, U. WEDIG, P. FUENTEALDA, AND H. STOLL, *J. Chem. Phys.* **84,** 5007 (1986).
40. M. MOSKOVITS AND T. MEJEAN, *Surf. Sci.* **156,** 756 (1985).